Electronic Supplementary Information

Upcycling Rust and Plastic Waste into Fe-MOF for Effective Energy Storage Application: Transformation of Trash to Treasure

Rakesh Deka[a], Diptangshu Datta Mal[a] and Shaikh M. Mobin[a,b,c]*

[a]Department of Chemistry, [b]Department of Biosciences and Bio-Medical Engineering, [c]Center of Advanced Electronics (CAE), Indian Institute of Technology Indore, Khandwa Road, Simrol, Indore 453552, India.

Corresponding Author: E-mail: xray@iiti.ac.in Tel: +91 731 6603 336

Physical measurements

All the reagents and solvents were purchased commercially and used without further purification. Thermogravimetric analysis (TGA) was recorded with a METTLER TOLEDO (TGA/DSC1) system through STARe software by a heating rate of 10 °C/min in an N_2 atmosphere up to 800 °C. For the Powder X-ray diffraction (PXRD) analysis, Cu Kα (0.154 nm) monochromatic radiation was used with a Bruker, D2-Phaser X-ray diffractometer. The morphologies were investigated by a field emission scanning electron microscope (FESEM, JEOL JSM-6500 F). Brunauer−Emmett−Teller (BET) surface area and Barrett−Joyner−Halenda (BJH) distribution determinations were conducted on an Autosorb iQ (Quantachrome Instruments, version 1.11). FT-IR experiment was performed by using Perkin Elmer-Spectrum Two with ATR mode. ^{1}H NMR (400 MHz) and ^{13}C NMR (100 MHz) spectra were recorded on a Bruker 400 MHz FT-NMR spectrometer at room temperature. ^{1}H NMR chemical shifts are reported in parts per million (ppm) relative to the solvent residual peak (DMSO-d_6, 2.5 ppm). ^{13}C NMR chemical shifts are reported relative to the solvent residual peak (DMSO-d_6, 39.52 ppm).

Experimental section

Materials

All the chemicals were taken from commercially available sources and further used without purification. The $FeCl_3.6H_2O$, Terephthalic acid, N, N-dimethylformamide (DMF), ethanol, Polyvinyl alcohol (PVA), and KOH were purchased from Finar and Merck chemicals. Moreover, the aqueous KOH solutions were prepared by using de-ionized water.

Synthesis of Fe-BDC(W)

For the synthesis of **Fe-BDC(W)**, we have taken a laboratory-used rusted iron container to produce metal salt precursor and a disposable polyethylene terephthalate (PET) bottle as a source of benzene dicarboxylic acid (linker). At first, the laboratory-used rusted iron container was scratched to get the iron rust powder. Later on, it was completely dissolved in 50% diluted HCl to get a mixture of iron chloride salts. The obtained mixture was treated with excess H_2O_2 to further oxidize to $FeCl_3$. The resulting solution was kept at room temperature to obtain the crystals of $FeCl_3$. $6H_2O$. On the other hand, the plastic bottles were cut into small pieces and washed with ethanol several times to wash away any impurities. It was further treated with 4N NaOH for 24h at 180 °C in hydrothermal conditions. The obtained solution is neutralized with concentrated HCl to get a white powder of benzene dicarboxylic acid. After that, we followed a reported pathway[1] with slight modification to produce **Fe-BDC(W)**. In a general reaction, $FeCl_3.6H_2O$ (5 mmol, 1.35 gm) and benzene dicarboxylic acid (2.47 mmol, 0.412 gm) was completely dissolved in 30 mL DMF and transferred to a Teflon-lined autoclave (40 mL) for 22h and heated at 110 °C. The obtained orange-colored powder was then washed several times with DMF, followed by deionized water and ethanol, and dried at room temperature to get pure **Fe-BDC(W)**.

Synthesis of Fe-BDC(C)

For comparison purposes, we have prepared another Fe-BDC(C) material with commercially available $FeCl_3.6H_2O$ and benzene dicarboxylic acid. The reaction procedure is the same as the **Fe-BDC(W)**.

Electrochemical study

Preparation of electrodes

For the electrochemical measurements, potentiostatic cyclic voltammetry (CV), galvanostatic charge-discharge (GCD), and electrochemical impedance spectroscopy (EIS) are used to evaluate the efficiency of **Fe-BDC(W)** and Fe-BDC(C). The electrochemical setup for all the measurements includes three conventional electrode systems. A platinum wire as a counter electrode, Ag/AgCl as the reference electrode, and carbon cloth (CC) as the working electrode. However, for the electrochemical measurements, the working electrode was prepared by drop casting of ethanolic dispersion of the active material on CC (200 μg of mass loading) and air dried at room temperature for further electrochemical study.

Efficiency evaluation

The specific capacitance (F g^{-1}) of the symmetric device was measured by using the following equation:[2]

$$C_s = \frac{I \times \Delta t}{m \times \Delta V} \quad \text{(S1)}$$

here *I/m* signifies current density, Δt, and ΔV convey the discharge time and potential window of the GCD profile.

Furthermore, for the asymmetric device, the energy density (E) and power density (P) were calculated by using the following equations:[3]

$$E = \frac{Cs}{2 \times 3.6} \times \Delta V^2 \quad \text{(S2)}$$

$$P = \frac{E}{\Delta t} \times 3600 \quad \text{(S3)}$$

here, C_s, ΔV and Δt signify the specific capacitance, potential window, and discharge time of the GCD profile, respectively.

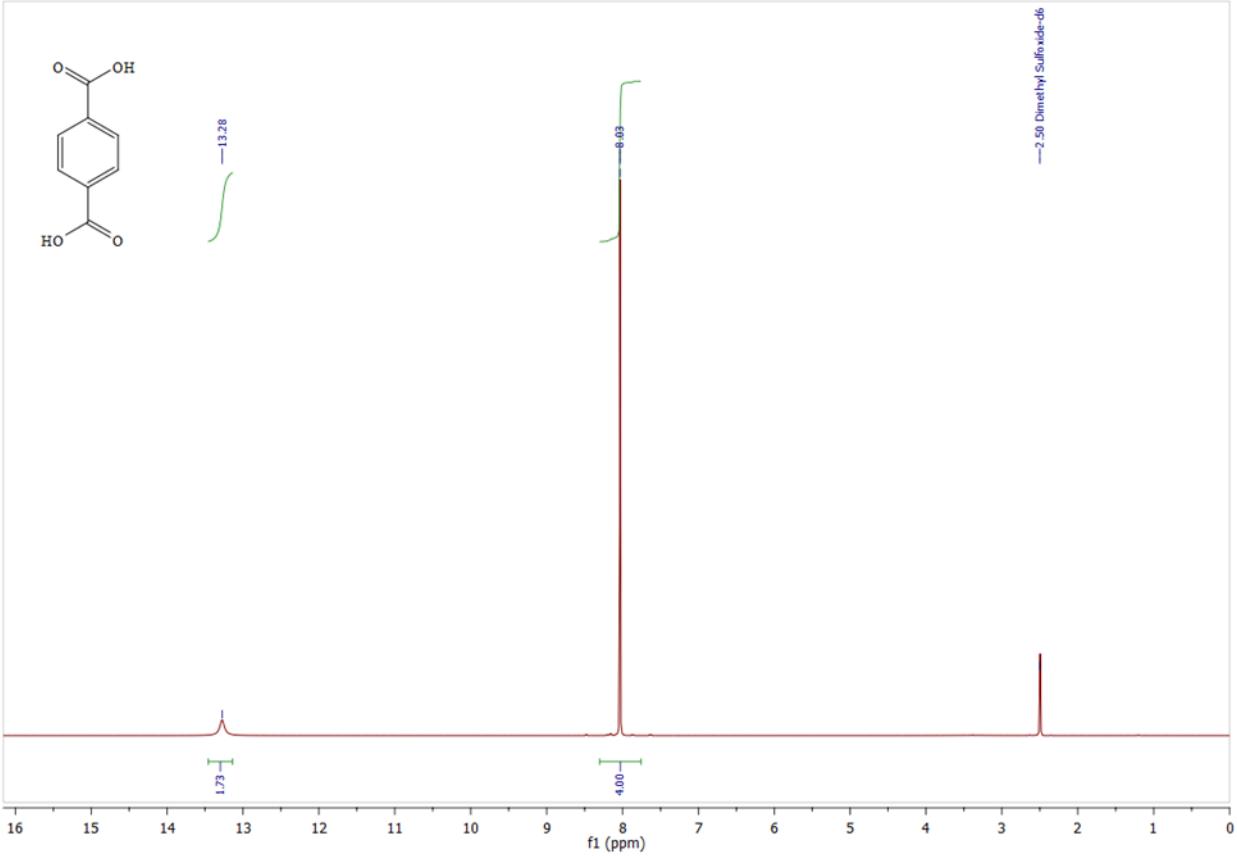

Fig. S1 ^{1}H NMR of PET-derived benzene dicarboxylic acid.

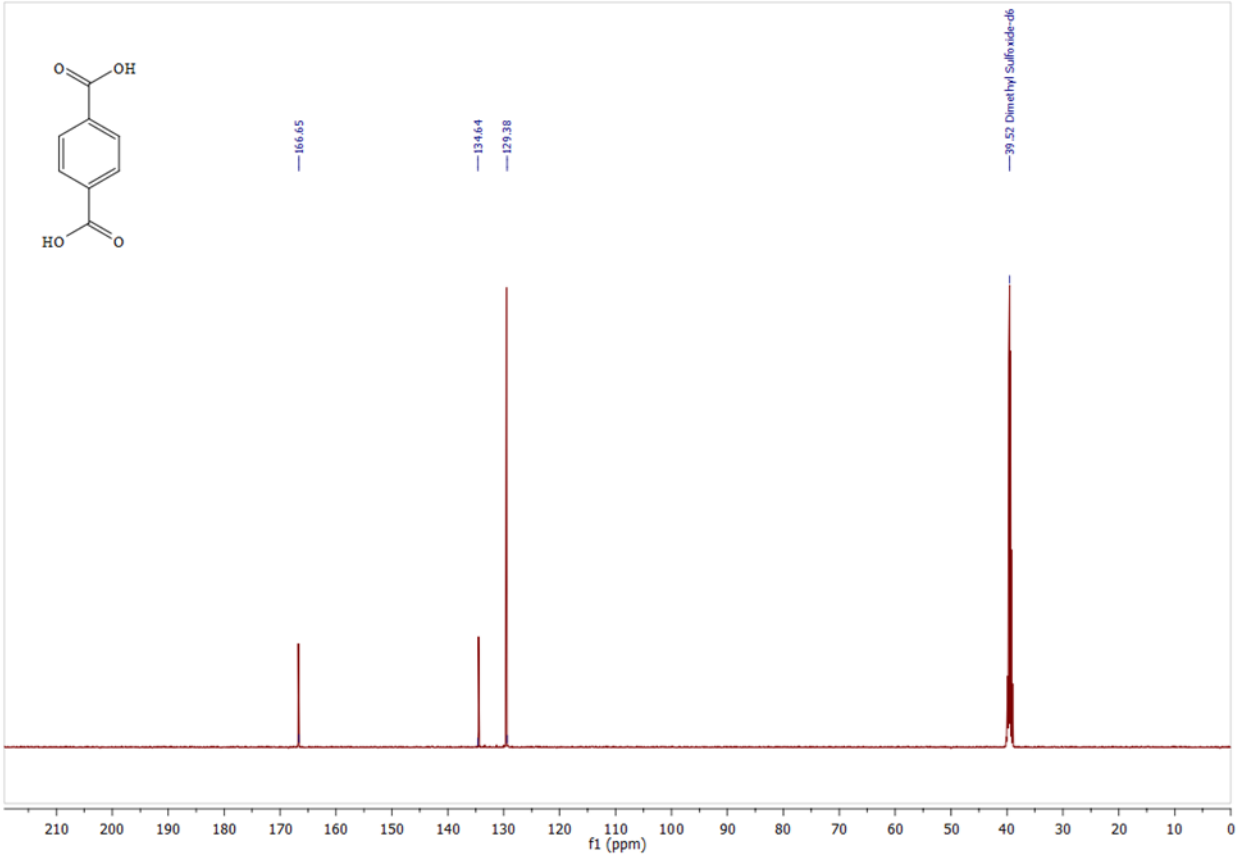

Fig. S2 ^{13}C NMR of PET-derived benzene dicarboxylic acid.

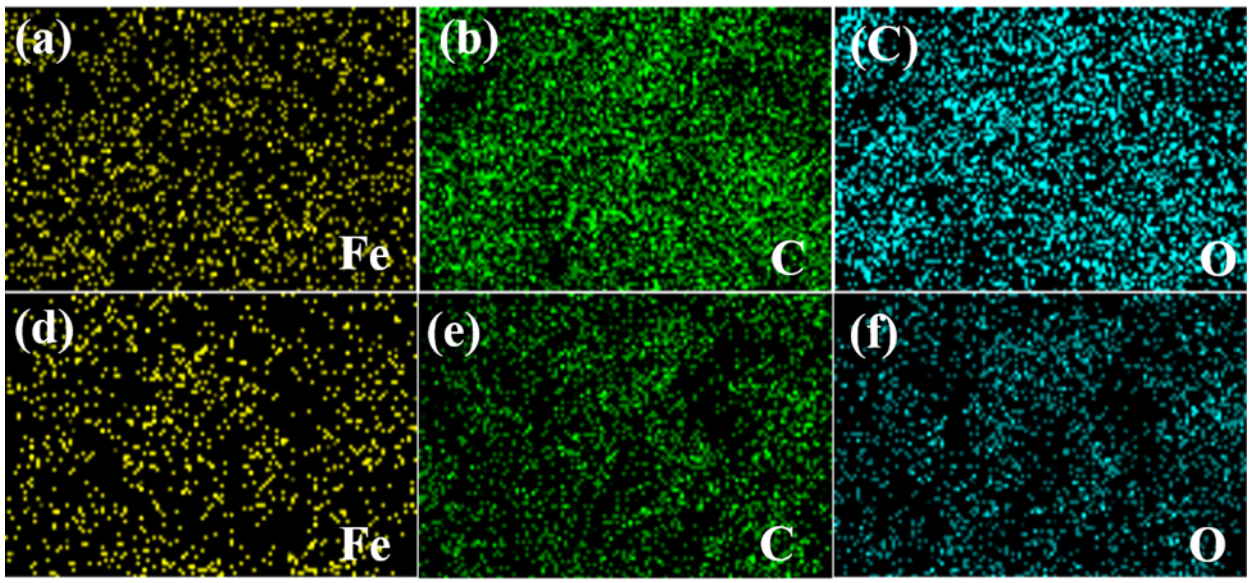

Fig. S3 (a-c) Elemental mapping of **Fe-BDC(W)**, (d-f) Elemental mapping of Fe-BDC(C).

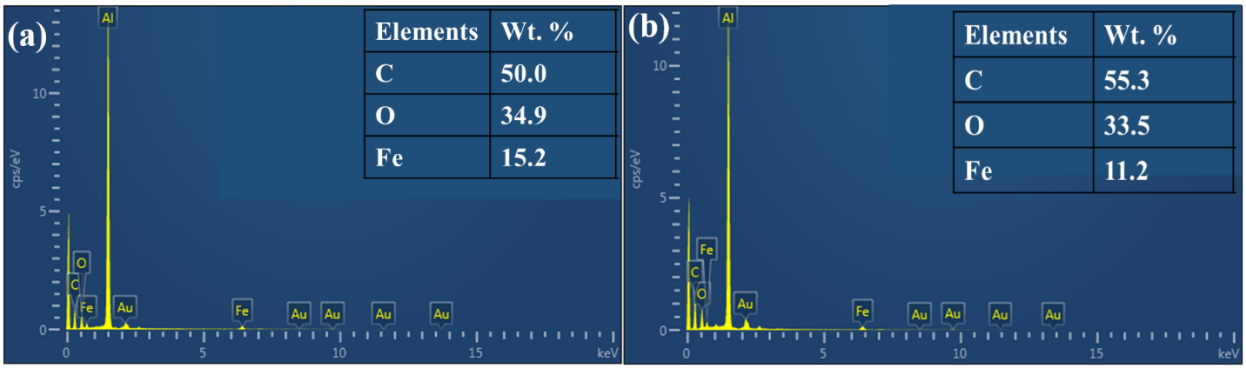

Fig. S4 (a) Elemental composition of Fe-BDC(C), (b) Elemental composition of **Fe-BDC(W)**.

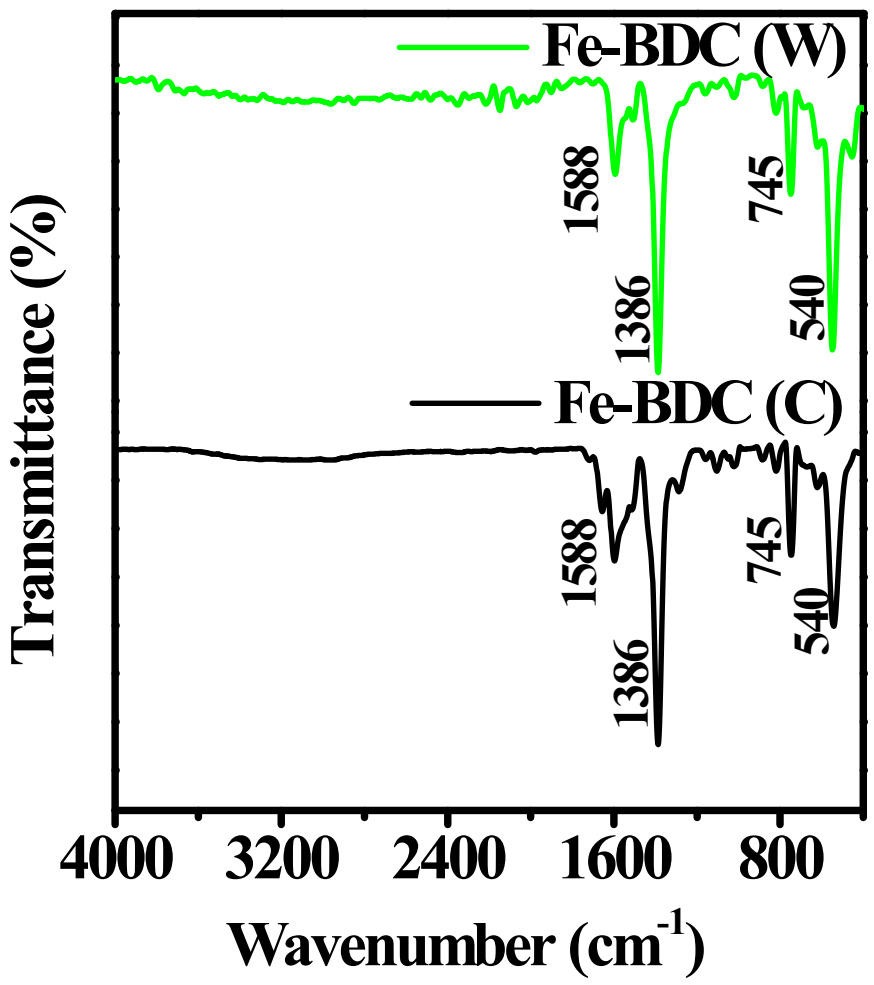

Fig. S5 FT-IR spectrum of **Fe-BDC(W)** and Fe-BDC(C).

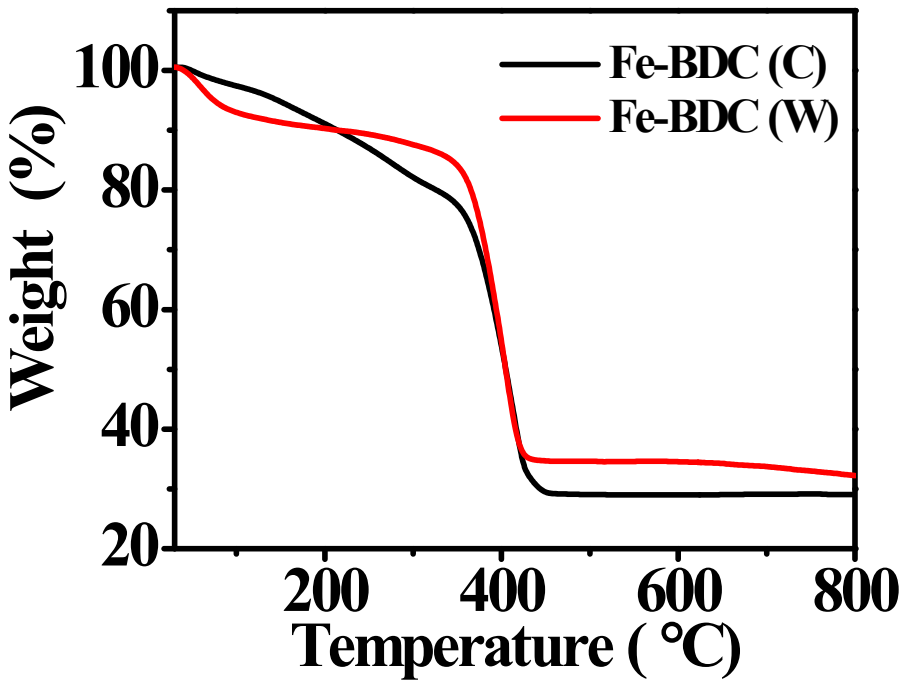

Fig. S6 Thermogravimetric analysis of Fe-BDC(C) and **Fe-BDC(W)**.

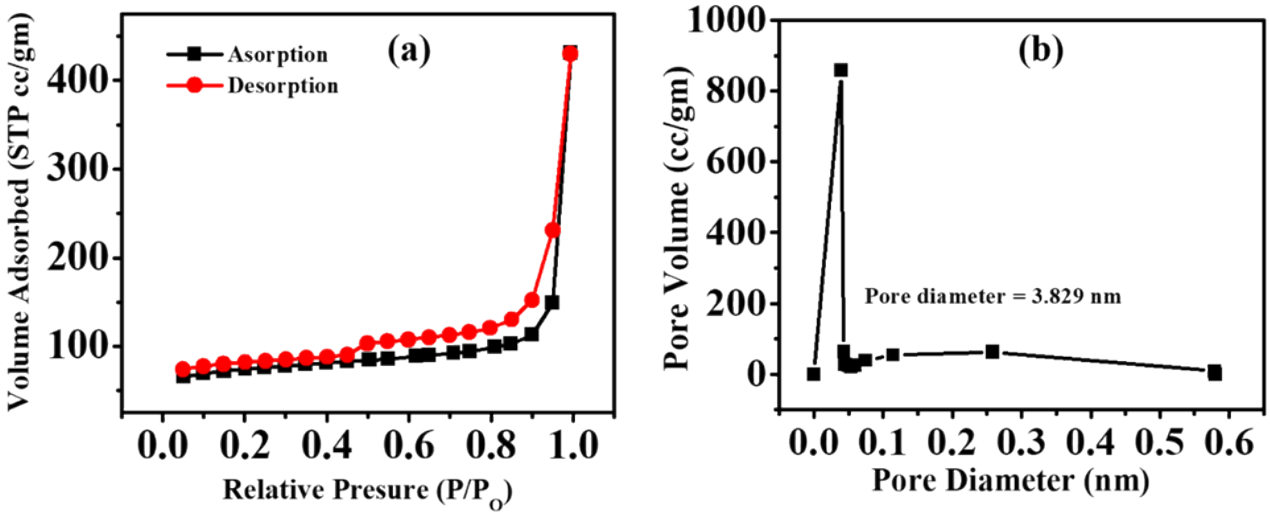

Fig. S7 (a) Nitrogen adsorption and desorption isotherms and (b) the corresponding pore size analysis of **Fe-BDC(W).**

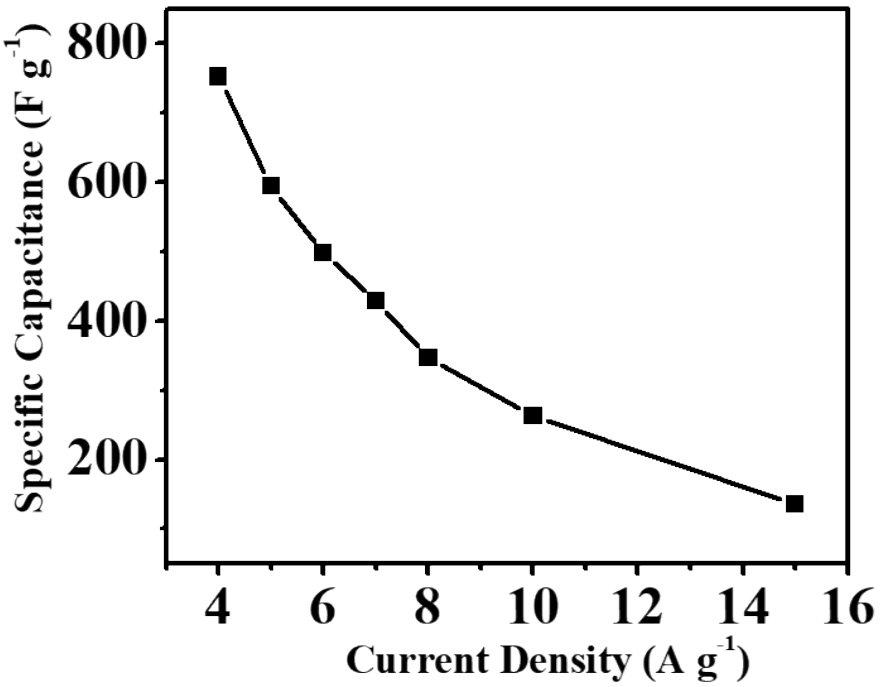

Fig. S8 Specific capacitance vs. Current density curve for **Fe-BDC(W)**.

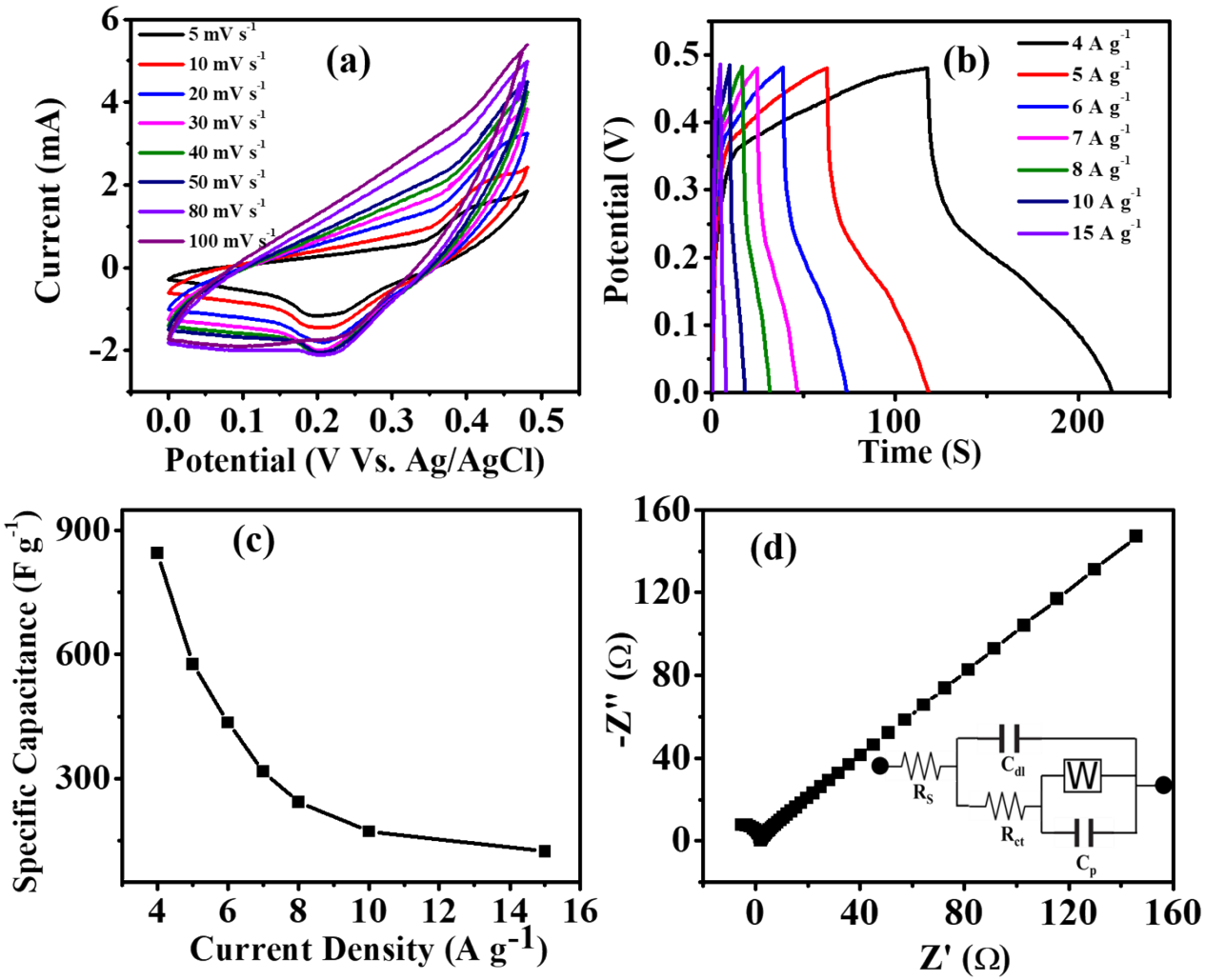

Fig. S9 (a) Cyclic Voltammetry at various scan rates, (b) GCD at different current densities, (c) Specific capacitance vs. Current density curve, and (d) Nyquist plot of Fe-BDC(C).

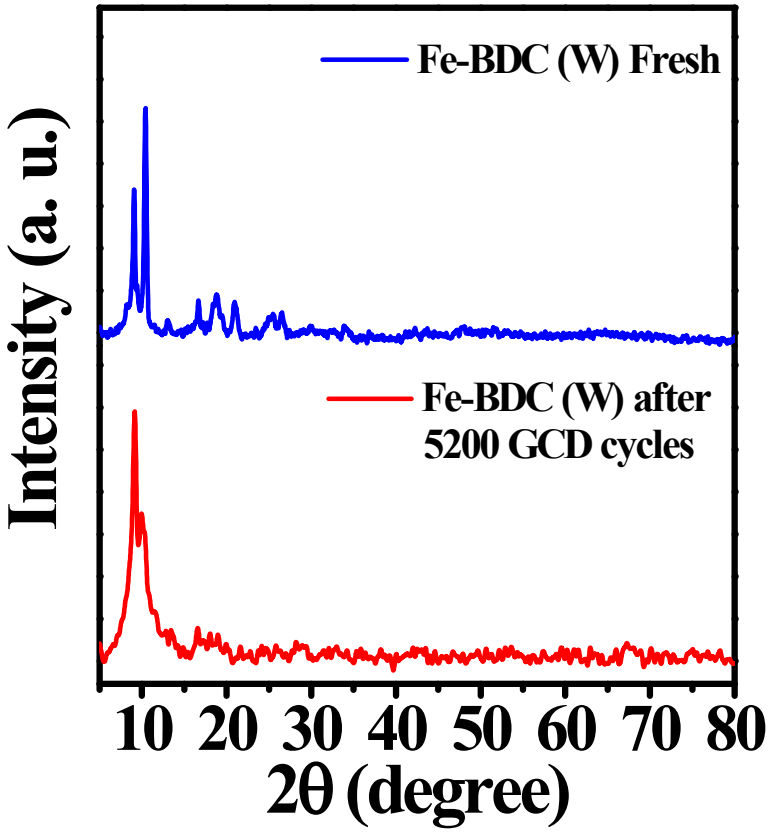

Fig. S10 PXRD pattern of **Fe-BDC(W)** before and after 5200 GCD cycles.

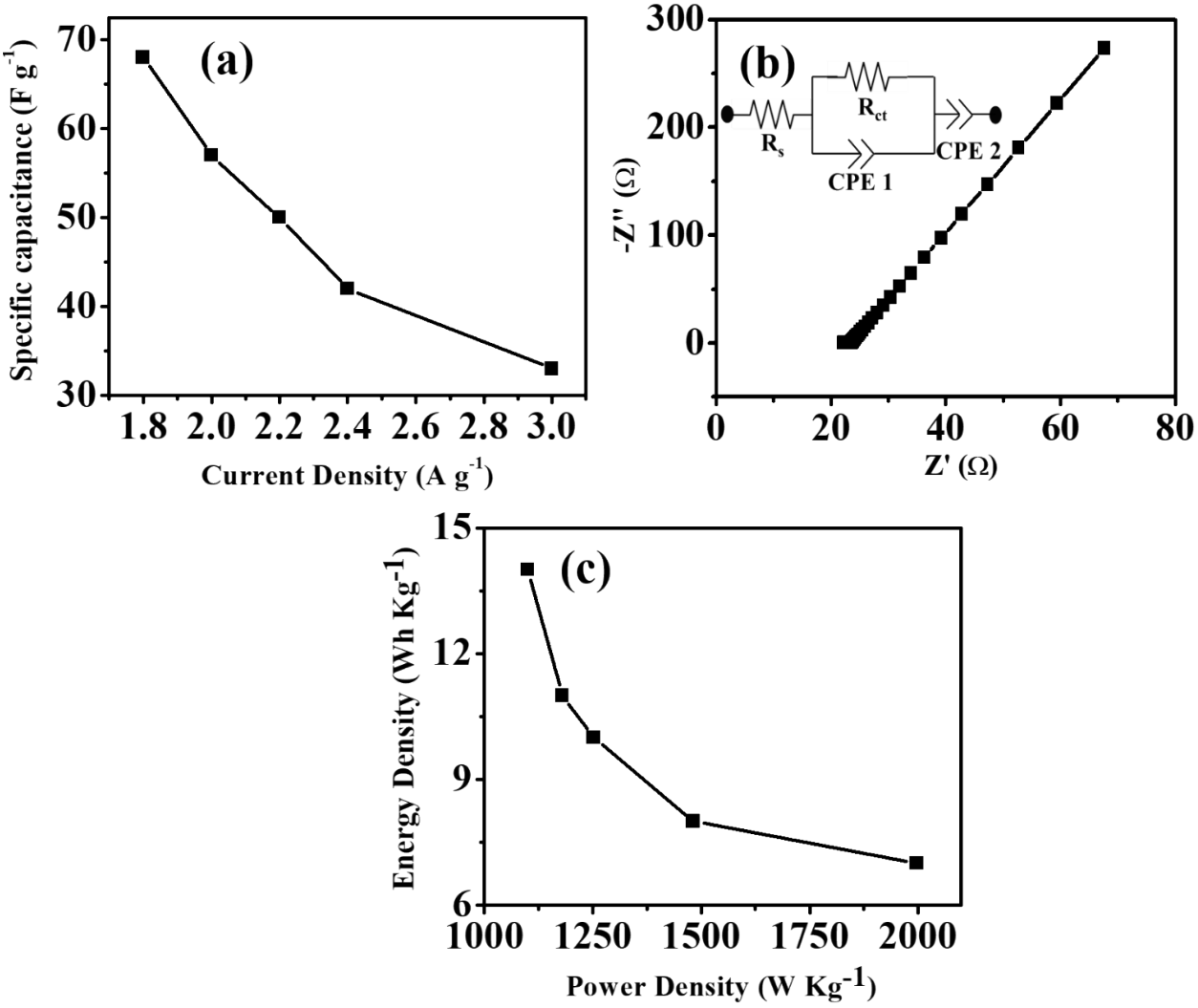

Fig. S11 (a) Specific capacitance vs. Current density, (b) Nyquist plot, and (c) Ragone plot of **Fe-BDC(W)** device.

Table S1 Comparison table of MOF-based material for supercapacitor application.

Sr. No.	Material	Electrolyte	Current Density (A g^{-1})	Specific Capacitance (F g^{-1})	Cyclic stability	Device Energy Density (Wh Kg^{-1})	Device Power Density (W Kg^{-1})	Ref.
1	Ni-MOF	3M KOH	1.4	988	96.5% after 5000 cycles	4.18 mW h cm^{-3}	231.2 mW cm^{-3}	[4]
2	Ni-based MOF	6M KOH	0.5	1127	90% after 3000 cycles.	-	-	[5]
3	Fe-MOF@AC	6M KOH	1	628.5	~82% after 10000 cycles	16.24	897.5	[6]
4	Ni/Co-MOF	2M KOH	1	758	75% after 5000 cycles	20.9	800	[7]
5	ZIF−PPy	1M Na_2SO_4	0.5	597.6	90.7% after 10,000 cycles	0.0113 mW h cm^{-2}	0.12 mW cm^{-2}	[8]
6	Ni-DMOF-ADC	2M KOH	1	552	~98% after 16,000 cycle	-	-	[9]
7	CuFeBTC /S-GNS	1M Na_2SO_4	0.5	1164.3	High cyclic stability after 10000 cycles	50.2	26973.13	[10]
8	MIL-88-Fe/GA	1M H_2SO_4	20	353	74.4% after 10000 cycles	36	588	[11]
9	Cd-MOF	1M KOH	4	647	78% after 10000 cycles	11.25	500	[2]
10	Ni-CP	7M KOH	3	802	95% after 5000 cycles	15	1137	[3]
11	NC-800	6M KOH	1	715	No degradation after 2500 cycles	-	-	[12]
12	Co-MOF	1M LiOH	1	206.76	98.5% after 1000 cycles	-	-	[13]
13	$[Co(bpdc)(H_2O)_2]H_2O$	0.5M LiOH	10 mV s^{-1}	179.2	No degradation after 1000 cycles	-	-	[14]
14	**Fe-BDC(W)**	**3 M KOH**	**4**	**752**	**83% after 5200 cycles**	**14**	**1100**	**This Work**

Table S2 Circuit fitting parameter for **Fe-BDC(W)** and Fe-BDC(C) for three electrode studies.

Elements	Fe-BDC(C)	**Fe-BDC(W)**
R_S (Ω)	12.4	13.9
R_{ct} (Ω)	15.2	15.7
C_{dl} (nF)	13.9	9.29
C_p (μF)	104	123
W (m Mho*s^(1/2))	4.21	6.06

Table S3 Circuit fitting parameter for asymmetric solid-state supercapacitor of **Fe-BDC(W)**.

Elements	**Fe-BDC(W)**
R_S (Ω)	22.1
R_{ct} (Ω)	1.43
CPE 1 (μMho*s^N)	54.3 (N= 0.787)
CPE 2 (mMho*s^N)	2.40 (N = 0.898)

References

1 Q. Xie, Y. Li, Z. Lv, H. Zhou, X. Yang, J. Chen and H. Guo, *Sci Rep*, 2017, **7**, 3316.

2 R. Deka, R. Rajak, V. Kumar and S. M. Mobin, *Inorg Chem*, 2023, **62**, 3084–3094.

3 R. Deka, V. Kumar, R. Rajak and S. M. Mobin, *Sustain Energy Fuels*, 2022, **6**, 3014–3024.

4 Y. Yan, P. Gu, S. Zheng, M. Zheng, H. Pang and H. Xue, *J Mater Chem A Mater*, 2016, **4**, 19078–19085.

5 J. Yang, P. Xiong, C. Zheng, H. Qiu and M. Wei, *J. Mater. Chem. A*, 2014, **2**, 16640–16644.

6 B. Ramasubramanian, C. Chinglenthoiba, X. Huiqing, N. Xiping, H. K. Hui, S. Valiyaveettil, S. Ramakrishna and V. Chellappan, *Surfaces and Interfaces*, 2022, **34**, 102397.

7 S. Gao, Y. Sui, F. Wei, J. Qi, Q. Meng, Y. Ren and Y. He, *J Colloid Interface Sci*, 2018, **531**, 83–90.

8 X. Xu, J. Tang, H. Qian, S. Hou, Y. Bando, Md. S. A. Hossain, L. Pan and Y. Yamauchi, *ACS Appl Mater Interfaces*, 2017, **9**, 38737–38744.

9 C. Qu, Y. Jiao, B. Zhao, D. Chen, R. Zou, K. S. Walton and M. Liu, *Nano Energy*, 2016, **26**, 66–73.

10 A. S. Rajpurohit, N. S. Punde and A. K. Srivastava, *J Colloid Interface Sci*, 2019, **553**, 328–340.

11 L. Liu, Y. Yan, Z. Cai, S. Lin and X. Hu, *Adv Mater Interfaces*, 2018, **5**, 1701548.

12 C. Young, J. Kim, Y. V. Kaneti and Y. Yamauchi, *ACS Appl Energy Mater*, 2018, **1**, 2007–2015.

13 D. Y. Lee, S. J. Yoon, N. K. Shrestha, S.-H. Lee, H. Ahn and S.-H. Han, *Microporous and Mesoporous Materials*, 2012, **153**, 163–165.

14 D. Y. Lee, D. v. Shinde, E.-K. Kim, W. Lee, I.-W. Oh, N. K. Shrestha, J. K. Lee and S.-H. Han, *Microporous and Mesoporous Materials*, 2013, **171**, 53–57.